 doi:10.20944/preprints202204.0261.v1

Using Objective Analysis for the Assimilation of Satellite Derived Aerosol Products to Improve $PM_{2.5}$ Predictions over Europe

Mounir Chrit[a,c], Marwa Majdi[a,b,c]

[a] *Laboratoire de Météorologie Dynamique (LMD)-IPSL, Sorbonne Université, CNRS UMR 8539, Ecole Polytechnique, Paris, France*
[b] *CEREA: joint laboratory École des Ponts ParisTech - EDF R&D, Université Paris-Est, 77455 Champs sur Marne, France*
[c] *now at Department of atmospheric sciences, University of North Dakota, Grand Forks, North Dakota, USA.*

Abstract

We used the objective analysis method in junction with the successive correction method to assimilate MODerate resolution Imaging Spectroradiometer (MODIS) Aerosol Optical Depth (AOD) data into Chimère model in order to improve the modeling of fine particulate matter ($PM_{2.5}$) concentrations and AOD field over Europe. A data assimilation module was developed to adjust the daily initial total column aerosol concentrations based on a forecast-analysis cycling scheme. The model is then evaluated during one-month winter period to examine how such data assimilation technique pushes the model results closer to surface observations. This comparison showed that the mean biases of both surface $PM_{2.5}$ concentrations and AOD field could be reduced from -34 to -15% and from -45 to -27%. The assimilation however leads to false alarms becasue of the difficulty to distribute AOD_{550} over different particles sizes. The impact of the influence radius is found to be small and depends on the density of satellite data. This work,

[1] mounir.chrit@und.edu, OrcID number: 0000-0002-9603-9019

 doi:10.20944/preprints202204.0261.v1

although preliminary, is important in terms of near-real time air quality forecasting using Chimère model and can be further developed to improve modeled $PM_{2.5}$ and ozone concentrations.

Keywords: $PM_{2.5}$, Aerosol Optical Depth, Data assimilation, MODIS, satellite data, Objective analysis.

1. Introduction

Air pollution in Europe has become a serious issue in recent years with the recorded concentrations of $PM_{2.5}$ (particlate matter of aeroynamical diameter smaller than 2.5 μm) (Bigi and Ghermandi, 2016; Barmpadimos et al., 2012). High concentrations of $PM_{2.5}$ can cause detrimental human health problems. $PM_{2.5}$ daily concentrations are very useful for health studies and regulations evaluation. Therefore, their accurate prediction and modeling is of paramount importance.

Chemistry-transport models are numerical tools to predict $PM_{2.5}$ concentrations on different scales. However, these models are uncertain. For example, Van Loon et al. (2004) confronted the simulated aerosol concentrations over Europe against surface observations and found that the root mean square error (RMSE) between both of them is about 10 $\mu g.m^{-3}$ and that the correlation rarely exceeds 50%. Additionally, Majdi et al. (2018) examined the uncertainties on air quality modeling, fire emissions parameters and $PM_{2.5}$ concentrations threshold exceedances over the Euro-Mediterranean region during two severe fire events in summer 2007 and revealed that the statistical dispersion for $PM_{2.5}$ concentrations can be as high as 75% depending on the chemical mechanisms, injection heights of fire emissions and model

 doi:10.20944/preprints202204.0261.v1

vertical resolution. He et al. (2014) used GEOS-Chem model to simulate Black Carbon (BC) over the Tibetan plateau and revealed that the model succeeded in capturing the seasonal variability of surface BC at rural sites but the observed wintertime peaks were not reproduced. Moreover, Prank et al. (2016) evaluated four regional CTMs using the measurements of PM chemical composition by the European Monitoring and Evaluation Program (EMEP) network. This study showed that the four models underestimate PM concentrations by 10-60% depending on the model and the simulation period and stressed the necessity of improving models performances. These discrepancies are due to the uncertainties related not only to meteorology (Chrit et al., 2018; Nilsson et al., 2001; Aan de Brugh et al., 2012; Ervens et al., 2011), chemistry (Chrit et al., 2018; Majdi et al., 2018; Feng et al., 2004), emissions (Chrit et al., 2018; Majdi et al., 2018; Roustan et al., 2010) but also initial conditions (Bocquet et al., 2015; Segers, 2002; Wu et al., 2008; Sandu et al., 2010). Different studies investigated the improvement of CTMs performance through the improvement of emissions (Chrit et al., 2018; Majdi et al., 2018), meteorological conditions (Chrit et al., 2018), chemical mechanisms (Chrit et al., 2018; Majdi et al., 2018) but other studies focused on improving the accuracy of the initial conditions for forecast applications (Hu et al., 2022; Sekiya et al., 2021; Liang et al., 2020; Schwartz et al., 2014).

Data assimilation (DA) is a powerful tool that exploits the available observations including airborne, ground-based or remote sensing observations in order to reduce model uncertainties on initial conditions. Several data assimilation approaches are available and range from statistical methods such as optimal interpolation (Lee et al., 2013), variational (Hu et al., 2022; Liang

 doi:10.20944/preprints202204.0261.v1

et al., 2020; Schwartz et al., 2014) to sequential such as Kalman filters and Ensemble Kalman Filters (EnKF) (Pagowski and Grell, 2012). For example, Liang et al. (2020) showed by comparing the control experiment involving no DA and an experiment involving DA of lidar Aerosol Extinction Coefficient (AEC) data that the 3-DVAR DA system was effective at assimilating lidar AEC data. While there were only five lidars within the simulation region, assimilating AEC data alone was still found to effectively improve the accuracy of the initial field, hence improving the forecast performance for $PM_{2.5}$ for more than 24h. The lidar AEC DA can reduce the RMSE of the surface $PM_{2.5}$ mass concentration in the initial field of the model by 17.6%. Although variational and sequential data assimilation techniques are advanced and complex, the Objective Analysis (OA), known also as optimal interpolation is very straightforward and computationally very portable (Wang et al., 2013; Tombette et al., 2009; Kumar et al., 2012). Agudelo et al. (2015) used both the objective analysis and EnKF techniques to improve PM_{10} estimates of AURORA model with ground-based measurements provided by IRCEL (the Belgian Interregional Environment Agency) over Belgium, Luxemburg, Germany and the Netherlands. They found that the model performance were improved better using OI than EnKF as the mean bias was reduced from -12.84 to 0.04 $\mu g.m^{-3}$ using OI and to 0.75 $\mu g.m^{-3}$ using EnKF. In addition, Kumar et al. (2012) used also AURORA model to assimilate ground level ozone O_3 and nitrogen dioxide NO_2 concentrations over Belgium. The evaluation over 70 AIRBASE stations showed that the correlation improved from 40 to 80% for O_3 and from 30 to 60% for NO_2 and the RMSE was reduced from 27.9 to 12.6$\mu g.m^{-3}$ for O_3 and from 17.4

Preprints (www.preprints.org) | NOT PEER-REVIEWED | Posted: 27 April 2022 doi:10.20944/preprints202204.0261.v1

to 11.0μg.m^{-3} for NO_2 during the month of June. During December, both the spatial correlation and the index of agreement of monthly means of both species concentrations improved considerably.

Therefore, by combining observations and model results, the OI can be used to improve initial conditions of CTMs and hence improve PM predictions either directly using surface concentrations or indirectly by comparing the aerosol optical depth (AOD) with the modeled one and make the correspondent adjustments (Tang et al., 2017, 2015). In fact, Kaufman et al. (2000) showed, based on 7 years comparison that AOD from MODIS is highly correlated with daily average AOD measured from Aerosol Robotic Network (AERONET) over more than 50 sites worldwide and even better correlated with hourly $PM_{2.5}$ measurements.

However, the indirect OI using observations from satellites is more relevant and useful because surface and airborne observations are not only sparse, but also spatially and temporally limited. For example, Tombette et al. (2009) assimilated particulate matter with a diameter lower than 10μm (PM_{10}) data with the BDQA (Base de Donnees sur la Qualité de lÁir: the French national data base for air quality that covers France) using optimal interpolation implemented in the chemistry-transport model Polair3D of the air quality modeling system Polyphemus and found that the statistics are not improved because the effects of D.A. are overshadowed and the concentrations become quickly close to the concentrations without D.A..

Satellite data has proven to be effective in improving model-derived AOD over the United States, Asia and the Indian ocean using OA technique (Adhikary et al., 2008; Park et al., 2011; Tang et al., 2017). For example, Tang

 doi:10.20944/preprints202204.0261.v1

et al. (2017) assimilated the AOD in Community Multi-scale Air Quality (CMAQ) modeling system and found that surface $PM_{2.5}$ concentrations biases over the Contiguous United States were reduced from -2.25 to 0.77 $\mu g.m^{-3}$. In addition, Tang et al. (2015) adjusted the initial conditions of the CMAQ model to assimilate MODIS AOD using OI and the model showed a great improvement as the bias of surface $PM_{2.5}$ and ozone was reduced from 7.14 to -0.11$\mu g.m^{-3}$ and from 2.54 ppbV to 1.06 ppbC respectively.

The aim of this paper is to show how satellite retrievals can be assimilated in the Chimère model using the OA technique. The model is then evaluated in terms of both modeled $PM_{2.5}$ concentrations and AOD improvements in order to quantify the spatio-temporal impact of assimilating MODIS AOD data on model performance.

The paper is structured as follow: section 2 describes the setups of the model and the DA system. Section 3 discusses the results of different numerical experiments and findings of different sensitivity studies.

2. Method overview and model setup

2.1. Development of the Forecast-Analysis Cycling scheme

The default configuration of the model without DA consists on taking the initial concentration of a given species i, given size section j and at a given time step from the output concentration computed from the previous time step. The configuration with DA suggested in this study is based on a "forecasting-analysis cycling scheme" and consists on using the model output AOD as the first guess and satellite AOD as input observations to generate the analysis of AOD, with which the model output concentrations are ad-

Preprints (www.preprints.org) | NOT PEER-REVIEWED | Posted: 27 April 2022 doi:10.20944/preprints202204.0261.v1

justed and fed back to the model as initial concentrations, instead of taking model output concentrations as the initial conditions as shown in Figure1.

The data assimilation system developed here is illustrated in Figure1 and can be summarized in a set of three steps:

1- The AOD is computed from the modeled aerosol concentrations and taken as a first guess AOD^{Chim} at 00 UTC every day.

2- The analysis of AOD field AOD^{ana} is computed at 00 UTC from AOD^{Chim} and the retrieved AOD^{obs} covering Europe during the prior day, using the OI described in section2.2.

3- The concentrations $C_{i,j}^{Chim}$ that refer to the concentration of each chemical component i of $PM_{2.5}$ at each size size bin j are updated, at 00 UTC using an adjustment ratio (AOD^{ana}/AOD^{Chim}) shown in section2.2 and the analysis of concentrations are computed $C_{i,j}^{ana}$ that refer to the analysis of the concentration of each component i of $PM_{2.5}$ at each size bin j.

For each daily job running, the data assimilation covers the hours during which the satellite observations are available.

2.2. Objective Analysis of Satellite-derived AOD

The Analysis-Forecast cycling scheme is based on adjusting the modeled concentrations with the ratio of the AOD analysis AOD^{ana} to modeled AOD^{Chim} as described by equation1. Th fraction $\frac{AOD^{ana}}{AOD^{chim}}$ is considered the same for all concentrations in the vertical column volume.

$$C_{i,j}^{ana} = C_{i,j}^{chim} \times \frac{AOD^{ana}}{AOD^{chim}} \tag{1}$$

The objective analysis of AOD at a grid point m is performed by successive corrcetions using equation 2. The successive correction method used in

Preprints (www.preprints.org) | NOT PEER-REVIEWED | Posted: 27 April 2022 doi:10.20944/preprints202204.0261.v1

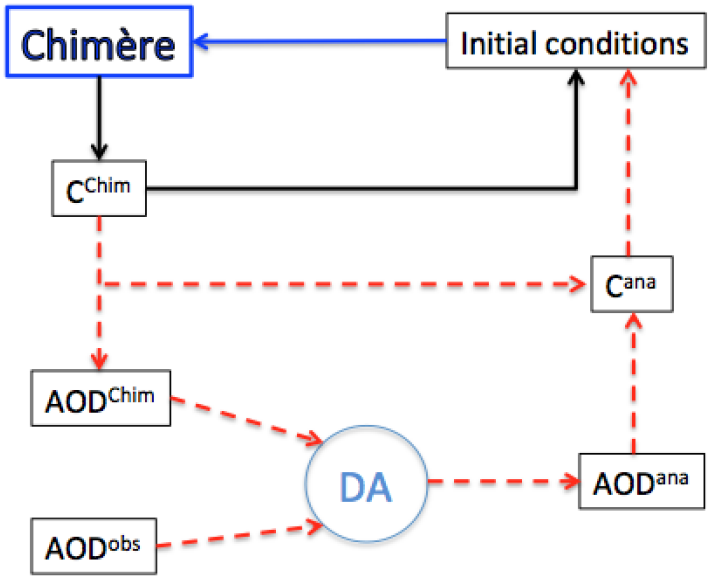

Figure 1: Illustration of the developed Analysis-Forecast cycling scheme. The blue arrow show the foreccast step. The black arrows refer to the basic configuration of the model. The red arrows refer to the developed data assimilation module.

this work is the Creesman scheme that uses satellite observations within a prescribed radius of influence as shown in figure2 and observations outside the influence radius are not used to assimilate the AOD field.

$$\begin{aligned} AOD^{ana}_{m,0} &= AOD^{Chim}_{m} \\ AOD^{ana}_{m,n+1} &= AOD^{ana}_{m,n} + \frac{\sum_{k=1}^{k=K_{m,n}} \alpha^{n}_{m,k}(AOD^{obs}_{k} - AOD^{ana}_{k,n})}{\sum_{k=1}^{k=K_{n}} \alpha^{n}_{m,k} + E^{2}} \end{aligned} \tag{2}$$

where AOD^{obs}_{k} is the k^{th} observation surrounding the grid point m, AOD^{Chim}_{m} is the modeled AOD using Chimère (background) at the grid point m, $AOD^{ana}_{m,n}$ is the n^{th} iteration estimation of AOD^{ana} at the grid point m and $AOD^{ana}_{k,n}$ is the n^{th} estimate of AOD^{ana} evaluated at the observation point k. $K_{m,n}$ refers to the index of the farest cell within the influence circle of radius equal

Preprints (www.preprints.org) | NOT PEER-REVIEWED | Posted: 27 April 2022 doi:10.20944/preprints202204.0261.v1

to the influence radius and centered on the grid point m. E^2 is an estimate of the ratio of the observation error to the first guess field error. This value is assumed to be 10%. $\alpha^n_{m,k}$ is a weight function which depends on how far the observation m is from the grid point k as shown equation3 where $r_{m,k}$ is the distance between an observation point k and a grid point m. The radius of influence R_n is allowed to vary with the iteration by a constant factor $R^2_{n+1} = \gamma\ R^2_n$. The factor γ is set to be less than 1 to reproduce the details in the observations field in the analysis field. Here, multiple values of the γ factor of 0.8, 0.5 and 0.3 were tested and is equal to 0.3 so the observation minus analysis increments (O-A) are located over observations location.

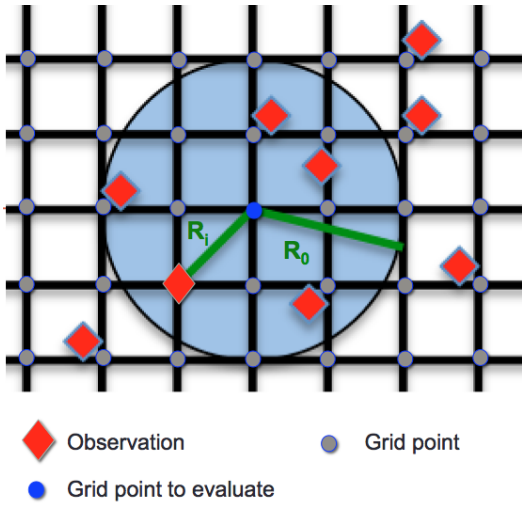

Figure 2: Objective analysis of satellite observation (red diamonds) onto a regulate grid shown in black using a circular influence (blue circle) as used in the Creesman scheme. R_0 is the radius of influence at the first iteration and R_i is the distance between the observation point and the grid point.

In this approach, selecting the proper values of the radius of influence is somewhat empirical and depends upon the data spacing and the desired

Preprints (www.preprints.org) | NOT PEER-REVIEWED | Posted: 27 April 2022 doi:10.20944/preprints202204.0261.v1

level of smoothing. Thiébaux and Pedder (1987) showed that a radius of influence is approximately twice the average spacing of the observations in a time when Tombette et al. (2009) used an influence radius of one mesh cell. These values tend to be a reasonable compromise between under-smoothing and over-smoothing. A radius of influence of one grid spacing is used as default and a sensitivity study to the radius of influence using a radius of one grid cell and two grid cells is conducted in section4.

$$\alpha_{m,k}^{n} = \begin{cases} \frac{R_n^2 - r_{m,k}^2}{R_n^2 + r_{m,k}^2} & r_{m,k}^2 < R_n^2 \\ 0 & r_{m,k}^2 \geq R_n^2 \end{cases} \tag{3}$$

Using this type of functions, the grid point values reflect the observations in areas of high observation density while in low-density areas, the grid values are closer to the first guess (modeled AOD).

2.3. Chimère model setup

Chimère model (Menut et al. (2013), ; http://www.lmd.polytechnique.fr/chimere) was run to simulate the concentrations of particles and their composition in 2013 over Europe. The domain covers the area from 14°W to 25°E in longitude and from 35°N to 58°N in latitude with a 0.5°× 0.5° of spatial resolution. There are 9 vertical levels up to 500hPa. The Chimèe model needs a set of gridded input data: meteorological data, sea salt, biogenic and anthropogenic emissions, land use parameters, initial and boundary conditions and deposition velocities.

Meteorology was obtained from the Weather Research and Forecasting model (WRF) regional model forced by NCEP (National Centers of Environmental Predictions, http://www.ncep.noaa.gov) with a base resolution of

 doi:10.20944/preprints202204.0261.v1

1°. The online coupling mode Chimère-WRF is used here with a feedback of the aerosol optical properties to induce a radiative forcing as shown in Briant et al. (2017).

Annual anthropogenic emissions of gases and particles were taken from the EMEP inventory for 2009. Temporalization of emissions is done according to temporal factors for each country provided by GENEMIS (GENEMIS, 1994).

Biogenic emissions are computed with the Model of Emissions and Gases and Aerosols from Nature (MEGAN) 2.1 (Guenther et al., 2006) with high-resolution emission factors and leaf area index (LAI) data. These emissions from biogenic sources include isoprene, limonene, α-pinene, β-pinene, humulene and ocimene. Sea-salt emissions were computed according to Monahan et al. (1986).

Boundary conditions were generated from the results of the Model for OZone And Related chemical Tracers (MOZART v4.0; Emmons et al. (2010)) available online at https://www.acom.ucar.edu/wrf-chem/mozart.shtml. Initial conditions of chemical species are taken from GOCART model (Chin et al., 2002).

The MELCHIOR2 (Derognat et al., 2003) mechanism was used to simulate the gas-phase chemistry.

Evaporation/condensation of semi-volatile species is represented with the algorithm of Pandis et al. (1993) using thermodynamic equilibria. Coagulation of particles is represented as in Debry et al. (2007). Thermodynamic equilibria are computed with the ISORROPIA II model (Fountoukis and Nenes, 2007) for inorganic compounds 10 bins for aerosol size distribution

Preprints (www.preprints.org) | NOT PEER-REVIEWED | Posted: 27 April 2022 doi:10.20944/preprints202204.0261.v1

and the SOA (secondary organic aerosols) scheme of Bessagnet et al. (2008) is used here. The Chimere aerosol module distributes aerosols in 10 size bins ranging from 40nm to 40 μm in a logarithmic sectional approach.

The Wesely (1989) aerosol dry deposition and Loosmore (2003) resuspension schemes were used. The online coupling with ISORROPIA model was used.

The basic chemical speciation includes elemental carbon, sulfate, nitrate, ammonium, sodium, chloride, dust, SOA (formed from biogenic and anthropogenic VOCs and primary organic aerosol) and the primary particulate matter other than ones mentioned above.

2.4. Observation data

2.4.1. MODIS data

MODIS products used in this study are a composite of AOD from MODIS TERRA (north to south transect at about 10:30 AM local time) and MODIS AQUA (south to north orbital transect about 1:30 PM local time) products. Both Terra- and Aqua-MODIS instruments view the entire Earth's surface every 1 to 2 days, acquiring data in 36 spectral bands ranging in wavelengths from 0.4 to 14.4μm. AOD retrievals were calculated at 0.55μm (AOD_{550}) and originally processed using MODIS data at a spatial resolution of 0.1° × 0.1°. The MODIS AOD field was projected to the 0.5° × 0.5° spatial longitude/latitude grid and happen to be only available in a subset of observation pixels due to multiple reflective surfaces and cloud contamination.

Preprints (www.preprints.org) | NOT PEER-REVIEWED | Posted: 27 April 2022 doi:10.20944/preprints202204.0261.v1

2.4.2. AERONET data

The AERONET (AErosol RObotic NETwork) photometers measurements (Holben et al., 2001, 1998), are used to characterize the observed AOD). The AOD data are recorded by numerous stations deployed around the world and hourly values are available in https://aeronet.gsfc.nasa.gov/new_web/aerosols.html. Several quality levels are proposed on the AERONET database. In this study, the level 2.0 AERONET AOD at 440 and 870 nm and ngstrm exponent ($AE_{440/870}$) (Dubovik and King, 2000) with an uncertainty estimated to less than 0.02 (Majdi et al., 2018; Holben et al., 1998) were used to derive AOD at 550 nm using logarithmic interpolation. If AOD value is not available at the 440, then AOD is not obtained at 550 nm. If the AOD at 870 nm is not available, the iterpolation is made between AOD at 440 and 1020 nm. The location of the stations are displayed in figure3.

2.4.3. AIRBASE data

AirBase (https://www.eea.europa.eu/data-and-maps/data/airbase-the-european-air-quality-database-8) gathers regulatory data reported by Member States of the European Union according to the air quality directives (AirBase, 2015). For this study, quality-controlled and assured hourly $PM_{2.5}$ data from both rural and urban background stations have been used. Figure3 shows the locations of the AirBase stations over Europe used here.

2.5. Statistical evaluation method

The statistical evaluation is based on a set of performance statistical indicators: the simulated mean ($\overline{s}$), the root mean square error (RMSE), the correlation coefficient, the mean fractional bias (MFB), the mean fractional

Preprints (www.preprints.org) | NOT PEER-REVIEWED | Posted: 27 April 2022 doi:10.20944/preprints202204.0261.v1

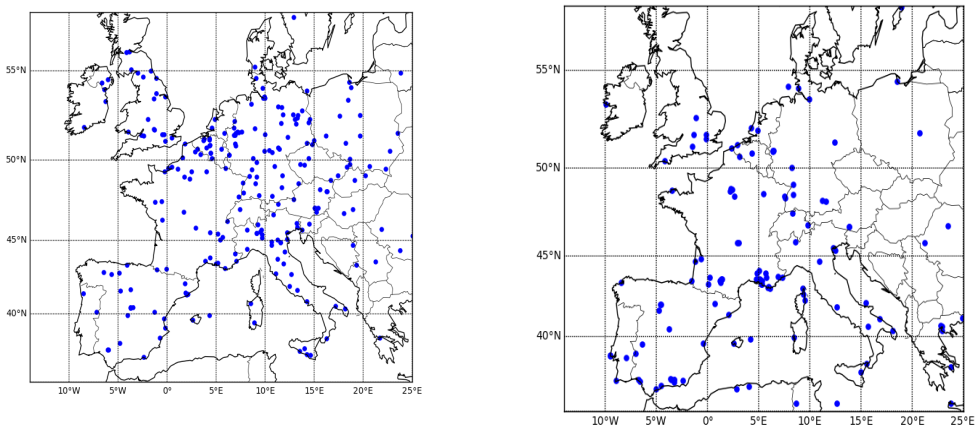

Figure 3: Maps of evaluation stations from AIRBASE network (184 stations) for $PM_{2.5}$ concentrations (right panel) and AERONET network (91 stations) for AOD (left panel)

error (MFE). They are defined in Table [1]. Based on the MFB and the MFE, Boylan and Russell (2006) proposed a performance and a goal evaluation criteria as detailed in Table [2].

Table 1: Definitions of the statistics used in this work. $(o_i)_i$ and $(c_i)_i$ are the observed and the simulated concentrations at time and location i, respectively. n is the number of data

Statistic indicator	Definition
Root mean square error (RMSE)	$\sqrt{\frac{1}{n}\sum_{i=1}^{n}(c_i - o_i)^2}$
Correlation (Corr)	$\frac{\sum_{i=1}^{n}(c_i - \bar{c})(o_i - \bar{o})}{\sqrt{\sum_{i=1}^{n}(c_i - \bar{c})^2}\sqrt{\sum_{i=1}^{n}(o_i - \bar{o})^2}}$
Mean fractional bias (MFB)	$\frac{1}{n}\sum_{i=1}^{n}\frac{c_i - o_i}{(c_i + o_i)/2}$
Mean fractional error (MFE)	$\frac{1}{n}\sum_{i=1}^{n}\frac{\mid c_i - o_i \mid}{(c_i + o_i)/2}$

Preprints (www.preprints.org) | NOT PEER-REVIEWED | Posted: 27 April 2022 doi:10.20944/preprints202204.0261.v1

Criteria	Performance criterion	Goal criterion
|MFB|	$\leq 60\%$	$\leq 30\%$
MFE	$\leq 75\%$	$\leq 50\%$

Table 2: Boylan and Russel criteria

2.6. An analysis example

An example of the calculation of the analysis of AOD field for the first simulation day of March 07^{th}, 2009 is shown in this section. All MODIS observations during a day are assimilated at 00 UTC: the MODIS observations at 1:30 Local Time are assimilated at 00UTC. The modeled, retrieved as well as the analysis of AOD field during that day are shown in figure4.

On March 07^{th} 2009, the MODIS data are not available over the whole European domain because of the cloud coverage during a wintertime day. The model tends to underestimate the AOD over areas where satellite data are available (a bias of -69% is found over the cells where MODIS data is available). The modeled AOD values do not exceed 0.3. The analysis of AOD field show higher values especially over Tunisia, Greece, south of France and Eastern Europe due to the impact of high observed AOD values.

A map of the adjustment ratio (AOD^{ana}/AOD^{Chim}) is shown in figure4.

Figure4 shows that this adjustment ratio locally exceeds 1.0 especially over regions where the satellite AOD are available.

3. Simulations experiments evaluation

Two simulations are performed with the same input data and parameterizations during the month of March 2009 which correspond to record pollution

Preprints (www.preprints.org) | NOT PEER-REVIEWED | Posted: 27 April 2022 doi:10.20944/preprints202204.0261.v1

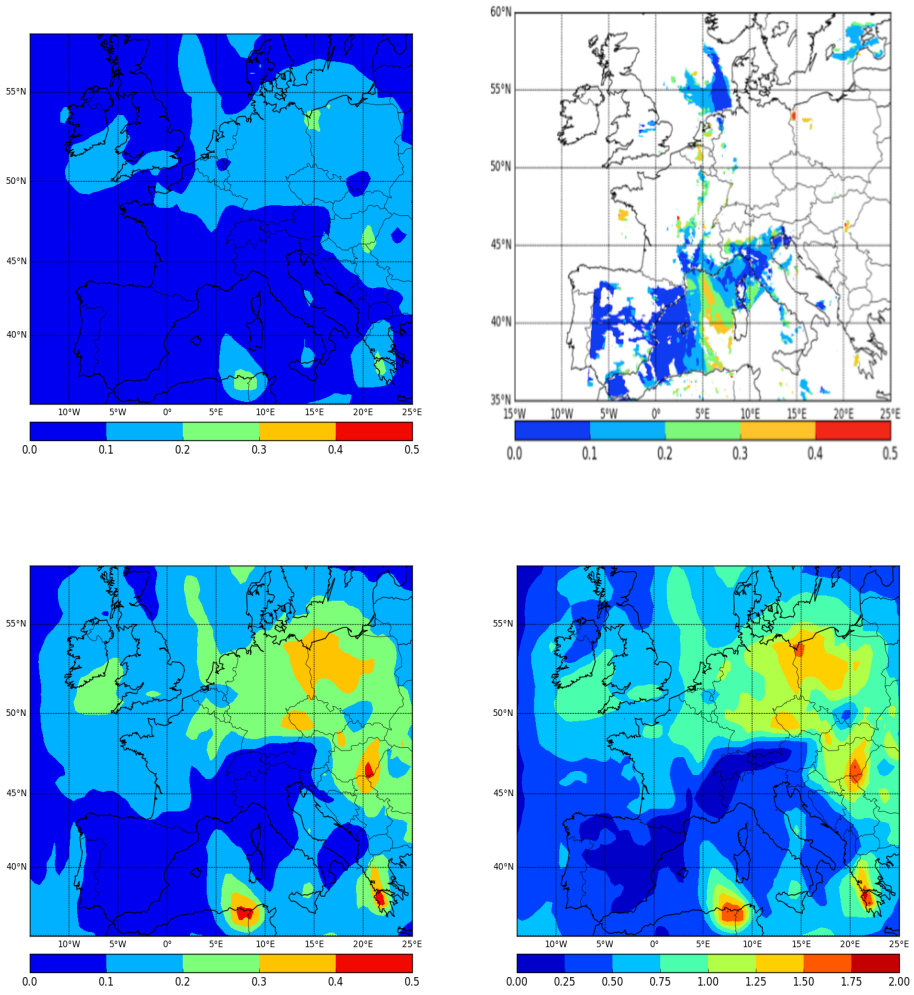

Figure 4: Upper left panel: Modeled AOD^{Chim} (first guess). Upper right panel: MODIS AOD_{obs} retrievals. Lower left panel: the analysis of AOD field AOD_{ana}. Lower right panel: Ratio of AOD analysis to the AOD first guess.

concentrations over Europe: the first one is the reference simulation without DA (called "Simulation without D.A."), the second one is run with the developed DA (called "Simulation with D.A."). Figure 5 shows maps of $PM_{2.5}$

Preprints (www.preprints.org) | NOT PEER-REVIEWED | Posted: 27 April 2022 doi:10.20944/preprints202204.0261.v1

concentrations and AOD field over Europe averaged over March 2009 and the relative difference between the two simulations in order to quantify the impact of OA on the model predictions.

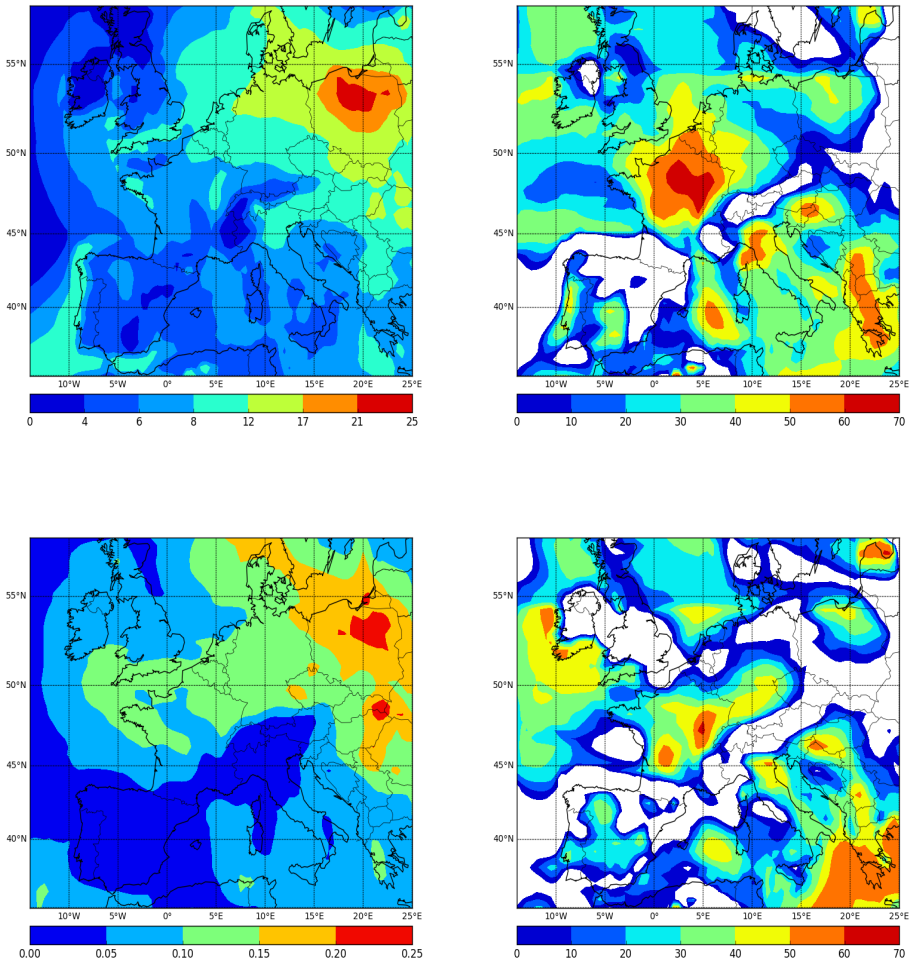

Figure 5: Maps of $PM_{2.5}$ concentrations (upper left), AOD field (lower left panel)and the relative difference between the simulations with and without objective analysis in terms of $PM_{2.5}$ concentrations (upper right panel) and AOD field (lower right panel)

Preprints (www.preprints.org) | NOT PEER-REVIEWED | Posted: 27 April 2022 doi:10.20944/preprints202204.0261.v1

$\overline{o} = 38.01\ \mu g.m^{-3}$	$\overline{s}$ [$\mu g.m^{-3}$]	RMSE [$\mu g.m^{-3}$]	Correlation [%]	MFB [%]	MFE [%]
Simulation without D.A.	20.89	30.05	40	-34	51
Simulation with D.A.	33.21	15.13	45	-15	39

Table 3: Statistics of model to AIRBASE measurements comparisons for hourly $PM_{2.5}$ concentrations during March 2009.

$\overline{o} = 0.37$	$\overline{s}$	RMSE	Correlation [%]	MFB [%]	MFE [%]
Simulation without D.A.	0.21	0.19	73	-45	55
Simulation with D.A.	0.30	0.11	78	-27	42

Table 4: Statistics of model to AERONET measurements comparisons for daily AOD during March 2009.

The effect of OA during the one-month period is significant. The main differences between the modeled concentrations of $PM_{2.5}$ and AOD with and without OA are located over France (∼50-60%) and the southern part of Europe (∼50-60%): the northern part of Italy, Balkans, south of Greece and over the Mediterranean.

The modeled $PM_{2.5}$ concentrations (resp. AOD) are compared against hourly surface observations from AirBase (resp. AERONET) network.

Using the default simulation without the DA, the modeled surface concentrations of $PM_{2.5}$ are significantly underestimated by a factor of about 47%(the measured and modeled means are 38.01 and 20.01 $\mu g.m^{-3}$ respectively). The goal criteria is not respected as the mean fractional bias and error are -34 and 51 % respectively. This underestimation is mainly due to the fact that the model highly underestimates $PM_{2.5}$ concentrations over the urban background stations but modeled $PM_{2.5}$ concentrations agree better

Preprints (www.preprints.org) | NOT PEER-REVIEWED | Posted: 27 April 2022 doi:10.20944/preprints202204.0261.v1

with the observed concentrations over the rural background. The reasons of this underestimation were explained by Terrenoire et al. (2015) who showed Chimère has more difficulty in reproducing the PM concentrations during winter, especially at urban background stations because the model is not able to correctly simulate the stable meteorological conditions that lead to high PM episodes (Stern et al., 2008).

During this winter month, $PM_{2.5}$ are mainly composed of primary organic compounds mainly emitted by industrial, traffic and biomass burning anthropogenic sectors. The hight concentrations are located over North Eastern Europe which is consistent with results found by Terrenoire et al. (2015).

Because of the OA, $PM_{2.5}$ concentrations increased by 59% as the simulated means moved from 20.89 to 33.21μg.m^{-3} and became closer to the observed mean (38.01μg.m^{-3}). The RMSE also decreased from 30.05 to 15.13μg.m^{-3}. The bias and error moreover, were reduced from -34 to -14% and from 51 to 39% respectively.

In addition, the model performance improved as the modeled $PM_{2.5}$ concentrations using OA respect the goal criterion in a time when the modeled concentrations without OA respects only the performance criterion. Tombette et al. (2009) evaluated the OA effect using Polyphemus model on both PM_{10} and $PM_{2.5}$ over 156 european stations, and found that PM_{10} concentrations increased by 7% and the bias was reduced from 55% to 49% and that over 8 european stations, $PM_{2.5}$ concentrations increased by a factor of 7%. Tang et al. (2015) also improved hourly $PM_{2.5}$ and ozone concentrations using OA over AIRNOW measurements as the mean bias improved from -7.14 to -0.11μg.m^{-3} and from 2.54 to 1.06 ppbV.

Preprints (www.preprints.org) | NOT PEER-REVIEWED | Posted: 27 April 2022 doi:10.20944/preprints202204.0261.v1

Similarly, the modeled AOD field over AERONET stations increased by a factor of 43% from 0.21 to 0.30. The correlation also slightly improved from 73 to 78%. Both the bias and error decreased from -45 to -27% and from 55 to 42%. While MODIS onboard Terra and Aqua pass at 10:30 and 1:30 local time respectively, AERONET can make a much wider range of measurements during different hours of the day which explains the high errors (42%)

Figure6 shows the scatter plots of hourly $PM_{2.5}$ concentrations and AOD modeled with and without the developed DA over AirBase and AERONET stations respectively.

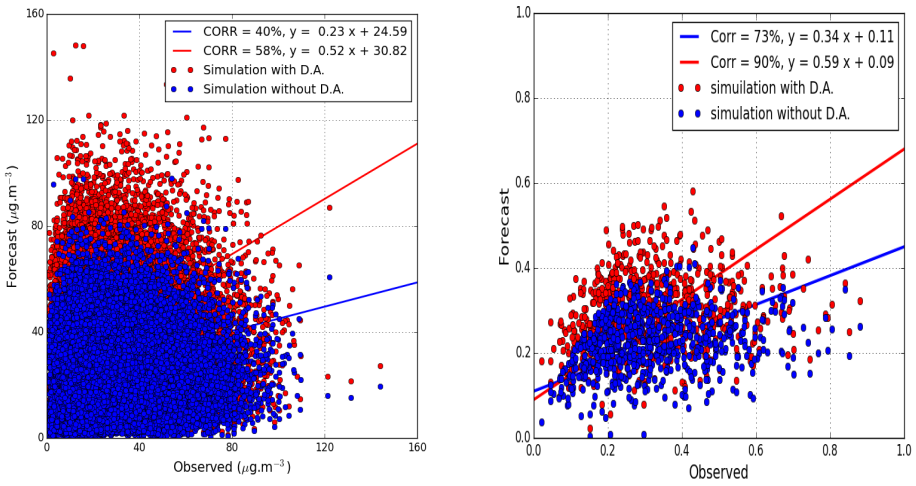

Figure 6: Scatter plots of the match-ups of model outputs surface $PM_{2.5}$ concentrations with AIRBASE observations (right panel), and AOD values with AERONET AOD (right panel)

The number of compared data in the AERONET network in is lower than the the compared data of AIRBASE because numerous missing data were found in AERONET data. The correlation moved from 40 to 58% and

Preprints (www.preprints.org) | NOT PEER-REVIEWED | Posted: 27 April 2022 doi:10.20944/preprints202204.0261.v1

the slope of the scatter plot increased from 0.23 to 0.52. The same result is found when it comes to the modeled AOD (the as the correlation increased from 73 to 90% and the slope of the scatter plot moved from 0.34 to 0.59. The analysis fields show an overestimation of the $PM_{2.5}$ concentrations. This overestimation (false alarms) can be explained by the fact that concentrations of PM with an aerodynamic diameter larger than 2.5μm are also sensitive to AOD_{550} and therefore are accounted for in equation 1. A better distribution of AOD by particles size should be added to avoid false alarms in the forecasting system in future studies.

3.1. Temporal impact of the OA

In order to evaluate the effectiveness of the MODIS AOD assimilation, the time scale for which the OA affects the concentrations is worth exploring because the OA operates on the initial conditions. Figure7 shows the hourly evolution of $PM_{2.5}$ concentrations averaged over all grid points where the relative difference is over 20% to better estimate the influence of the DA. Figure7 shows that the effect of OA lasts nearly 13 hours which is comparable to the temporal impact found by Tombette et al. (2009) using OA along with Polyphemus model over Europe. After 13 hours, MODIS data impact on the modeled concentrations is low because the impact of the regional transport and local emissions start overshadowing the assimilation impact.

4. Sensitivity to the Creesman influence radius

The performance of the OA is tested using two different influence radii. A first (resp. second) simulation using an influence radius R_1 (R_2) equal to (is twice) the grid cell spacing which corresponds to 0.5° (1°).

Preprints (www.preprints.org) | NOT PEER-REVIEWED | Posted: 27 April 2022 doi:10.20944/preprints202204.0261.v1

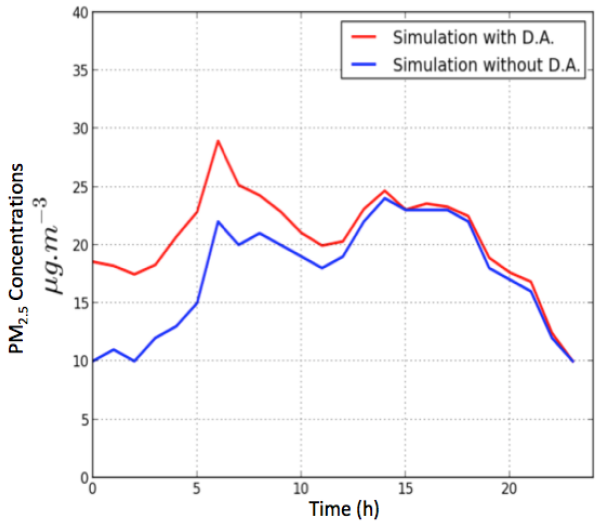

Figure 7: Daily profile of $PM_{2.5}$ concentrations averaged temporally over the one-month simulation period and on cells on which the $PM_{2.5}$ relative difference is higher than 20%

Table 5 shows the temporal and spatial sum of relative differences between the simulations with OA computed with R_1 and R_2 respectively over the cells where the effect of OI exceeds 20%. The comparison shows that the model performance is slightly sensitive to the influence radius value: the relative difference between the two simulations do not exceed 10.5 (12.3)% for $PM_{2.5}$ concentrations (AOD). This may be due to the low satellite observation density during winter because of dense cloud coverage. The results are expected to be more sensitive to influence radius if the satellite data were of better quality or during summertime.

The comparison of the two simulations against AirBase and AERONET data show that simulation with a radius of influence equal to the grid cell predicts $PM_{2.5}$ and AOD that have a better agreement with observations. The simulated mean of $PM_{2.5}$ concentrations (AOD) 33.21μg.m^{-3} (0.30) are

Preprints (www.preprints.org) | NOT PEER-REVIEWED | Posted: 27 April 2022 doi:10.20944/preprints202204.0261.v1

Influence radius	Relative difference (%)
$PM_{2.5}$	10.2
AOD	12.3

Table 5: Temporal and spatial sum of relative differences between the simulations whereby the influence radius is set to twice and equal to the average spacing of observations

$\overline{o} = 38.01\ \mu g.m^{-3}$	$\overline{s}$ [$\mu g.m^{-3}$]	RMSE [$\mu g.m^{-3}$]	Correlation [%]	MFB [%]	MFE [%]
Simulation with DA (R_1)	33.21	15.13	45	-15	39
Simulation with DA (R_2)	29.44	20.71	40	-31	51

Table 6: Statistics of hourly simulated $PM_{2.5}$ concentrations with DA using two influence radii R_1 and R_2 to AIRBASE measurements comparisons during March 2009.

$\overline{o} = 0.37$	$\overline{s}$	RMSE	Correlation [%]	MFB [%]	MFE [%]
Simulation with DA (R_1)	0.30	0.11	78	-27	42
Simulation with DA (R_2)	0.25	0.31	65	-54	72

Table 7: Statistics of hourly simulated AOD with DA using two influence radii R_1 and R_2 to AERONET measurements comparisons for daily AOD during March 2009.

 doi:10.20944/preprints202204.0261.v1

closer to the observed means 38.01μg.m^{-3} (0.37). Besides, the goal criteria is respected with analysis $PM_{2.5}$ concentration field simulated using R_1.

5. Conclusion

In this study, we tested the assimilation method of objective analysis to adjust Chimère's initial conditions for the simulation of $PM_{2.5}$ and AOD_{550} over Europe during March 2009. The base model underestimated surface $PM_{2.5}$ concentrations and AOD field because of the low resolution and uncertainties on meteorology and emissions. The objective analysis assimilation was able to correct the aerosol concentrations and AOD fields. However, the impact of adjusting initial conditions can be overshadowed by the local emissions and local winds as it lasted for 13h.

Assimilating data from elevated levels or airborne measurements, although occasionally available, can be used to sharpen the adjustment of initial conditions and would improve $PM_{2.5}$ concentration and AOD field as it represents the loading of the aerosol column.

Future works could focus on investigating the OA impact on finer-resolution simulations, better describing the background and observation covariance matrices, using more complex data assimilation techniques like 4D-var and ensemble Kalman filter, better describing the emissions using a top-down approach (inverse modeling), combining the use of satellite data with ground based or airborne observations of the aerosol chemical composition (organics, sulfate, nitrate, sea-salts, etc). The use of lidar observations could furthermore be very beneficial to improve the vertical distribution of aerosols.

Acknowledgements

This research was funded by Sorbonne University.

References

Adhikary, B., Kulkarni, S., Dallura, A., Tang, Y., Chai, T., Leung, L.R., Qian, Y., Chung, C.E., Ramanathan, V., Carmichael, G.R.. A regional scale chemical transport modeling of asian aerosols with data assimilation of aod observations using optimal interpolation technique. Atmos Env 2008;42:8600âĂŞ8615. doi:10.1016/j.atmosenv.2008.08.031.

Agudelo, O.M., Viaene, P., De Moor, B.. Improving the pm_{10} estimates of the air quality model AURORA by using Optimal Interpolation. Atmos Env 2015;48:1154–1159. URL: https://doi.org/10.1016/j.ifacol.2015.12.287. doi:10.1016/j.ifacol.2015.12.287.

AirBase, E.. The european air quality database, version 8 2015;URL: http://www.eea.europa.eu/data-and-maps/data/airbase-the-european-air-quality-dat (Accesses 13.01.15).

Barmpadimos, I., Keller, J., Oderbolz, D., Hueglin, C., Prévôt, A.S.H.. One decade of parallel fine ($pm_{2.5}$) and coarse (pm_{10} – $pm_{2.5}$) particulate matter measurements in europe: trends and variability. Atmos Chem Phys 2012;12(7):3189–3203. URL: https://www.atmos-chem-phys.net/12/3189/2012/. doi:10.5194/acp-12-3189-2012.

Bessagnet, B., Menut, L., Curci, G., Hodzic, A., Guillaume, B., Liousse, C., Moukhtar, S., Pun, B., Seigneur, C., Schulz, M.. Regional modeling of carbonaceous aerosols over Europe-focus on secondary organic aerosols. J Atmos Chem 2008;61:175–202. doi:10.1007/s10874-009-9129-2.

Bigi, A., Ghermandi, G.. Trends and variability of atmospheric $pm_{2.5}$ and $pm_{10–2.5}$ concentration in the po valley, italy. Atmos Chem Phys 2016;16(24):15777–15788. URL: https://www.atmos-chem-phys.net/16/15777/2016/. doi:10.5194/acp-16-15777-2016.

Bocquet, M., Elbern, H., Eskes, H., Hirtl, M., Žabkar, R., Carmichael, G.R., Flemming, J., Inness, A., Pagowski, M., Pérez Camaño, J.L., Saide, P.E., San Jose, R., Sofiev, M., Vira, J., Baklanov, A., Carnevale, C., Grell, G., Seigneur, C.. Data assimilation in atmospheric chemistry models: current status and future prospects for coupled chemistry meteorology models. Atmos Chem Phys 2015;15(10):5325–5358. URL: https://www.atmos-chem-phys.net/15/5325/2015/. doi:10.5194/acp-15-5325-2015.

Boylan, J.W., Russell, A.G.. PM and light extinction model performance metrics, goals, and criteria for three-dimensional air quality models. Atmos Env 2006;40(26):4946–4959. doi:10.1016/j.atmosenv.2005.09.087.

Briant, R., Tuccella, P., Deroubaix, A., Khvorostyanov, D., Menut, L., Mailler, S., Turquety, S.. Aerosol–radiation interaction modelling using online coupling between the wrf 3.7.1 meteorological model and the chimere 2016 chemistry-transport model, through the

oasis3-mct coupler. Geoscientific Model Development 2017;10(2):927–944. URL: https://gmd.copernicus.org/articles/10/927/2017/. doi:10.5194/gmd-10-927-2017.

Aan de Brugh, J.M.J., Henzing, J.S., Schaap, M., Morgan, W.T., van Heerwaarden, C.C., Weijers, E.P., Coe, H., Krol, M.C.. Modelling the partitioning of ammonium nitrate in the convective boundary layer. Atmos Chem Phys 2012;12(6):3005–3023. URL: https://www.atmos-chem-phys.net/12/3005/2012/. doi:10.5194/acp-12-3005-2012.

Chin, M., Ginoux, P., Kinne, S., Torres, O., Holben, B.N., Duncan, B.N., Martin, R.V., Logan, J.A., Higurashi, A., Nakajima, T.. Tropospheric Aerosol Optical Thickness from the GOCART Model and Comparisons with Satellite and Sun Photometer Measurements. J Atmos Sci 2002;59:461âĂŞ483. URL: https://doi.org/10.1175/1520-0469(2002)059<0461:TAOTFT>2.0.CO;2. doi:10.1175/1520-0469(2002)059<0461:TAOTFT>2.0.CO;2.

Chrit, M., Sartelet, K., Sciare, J., Majdi, M., Nicolas, J., Petit, J.E., Dulac, F.. Modeling organic aerosol concentrations and properties during winter 2014 in the northwestern mediterranean region. Atmos Chem Phys Discuss 2018a;2018:1–28. URL: https://www.atmos-chem-phys-discuss.net/acp-2018-149/. doi:10.5194/acp-2018-149.

Chrit, M., Sartelet, K., Sciare, J., Pey, J., Nicolas, J.B., Marchand, N., Freney, E., Sellegri, K., Beekmann, M., Du-

lac, F.. Aerosol sources in the western mediterranean during summertime: a model-based approach. Atmos Chem Phys 2018b;18(13):9631–9659. URL: https://www.atmos-chem-phys.net/18/9631/2018/. doi:10.5194/acp-18-9631-2018.

Debry, É., Fahey, K., Sartelet, K., Sportisse, B., Tombette, M.. Technical Note: A new SIze REsolved Aerosol Model (SIREAM). Atmos Chem Phys 2007;7(6):1537–1547. doi:10.5194/acp-7-1537-2007.

Derognat, C., Beekmann, M., Baeumle, M., Martin, D., Schmidt, H.. Effect of biogenic volatile organic compound emissions on tropospheric chemistry during the atmospheric pollution over the paris area (esquif) campaign in the ile-de-france region. J Geophys Res 2003;108. doi:10.1029/2001JD001421.

Dubovik, O., King, M.D.. A flexible inversion algorithm for retrieval of aerosol optical properties from sun and sky radiance measurements. Journal of Geophysical Research: Atmospheres 2000;105(D16):20673–20696. URL: https://agupubs.onlinelibrary.wiley.com/doi/abs/10.1029/2000JD900282. doi:https://doi.org/10.1029/2000JD900282. arXiv:https://agupubs.onlinelibrary.wiley.c

Emmons, L.K., Walters, S., Hess, P.G., Lamarque, J.F., Pfister, G.G., Fillmore, D., Granier, C., Guenther, A., Kinnison, D., Laepple, T., Orlando, J., Tie, X., Tyndall, G., Wiedinmyer, C., Baughcum, S.L., Kloster, S.. Description and evaluation of the model for ozone and related chemical tracers, version 4

(mozart-4). GeoscientificModelDevelopment 2010;3(1):43-67. URL: http://www.geosci-model-dev.net/3/43/2010/. doi:10.5194/gmd-3-43-2010.

Ervens, B., Turpin, B.J.,, , Weber, R.J.. Secondary organic aerosol formation in cloud droplets and aqueous particles (aqSOA): a review of laboratory, field and model studies. Atmos Chem Phys 2011;11:11069-11102. doi:10.5194/acp-11-11069-2011.

Feng, Y., Penner, J.E., Sillman, S., Liu, X.. Effects of cloud overlap in photochemical models. J Geophys Res 2004;109:D04310. doi:10.1029/2003JD004040.

Fountoukis, C., Nenes, A.. Isorropia ii: a computationally efficient thermodynamic equilibrium model for K^+ - Ca^{2+} - Mg^{2+} - $NH_4{}^+$ - Na^+ - $SO_4{}^{2-}$ - $NO_3{}^-$ - Cl^- - H_2O aerosols. AtmosphericChemistryandPhysics 2007;7(17):4639-4659. URL: https://www.atmos-chem-phys.net/7/4639/2007/. doi:10.5194/acp-7-4639-2007.

GENEMIS, . Genemis (generation and evaluation of emission) data. Technical Report, EUROTRAC 1994;Annual report.

Guenther, A., Karl, T., Harley, P., Wiedinmyer, C., Palmer, P.I., Geron, C.. Estimates of global terrestrial isoprene emissions using MEGAN (Model of Emissions of Gases and

Aerosols from Nature). Atmos Chem Phys 2006;6(11):3181-3210. doi:10.5194/acp-6-3181-2006.

He, C., Li, Q.B., Liou, K.N., Zhang, J., Qi, L., Mao, Y., Gao, M., Lu, Z., Streets, D.G., Zhang, Q., Sarin, M.M., Ram, K.. A global 3-d ctm evaluation of black carbon in the tibetan plateau. Atmos Chem Phys 2014;14(13):7091-7112. URL: https://www.atmos-chem-phys.net/14/7091/2014/. doi:10.5194/acp-14-7091-2014.

Holben, B., Eck, T., Slutsker, I., Tanré, D., Buis, J., Setzer, A., Vermote, E., Reagan, J., Kaufman, Y., Nakajima, T., Lavenu, F., Jankowiak, I., Smirnov, A.. AERONET : A federated instrument network and data archive for aerosol characterization. Remote Sens Environ 1998;66:1-16. doi:10.1016/S0034-4257(98)00031-5.

Holben, B.N., TanrÃĽ, D., Smirnov, A., Eck, T.F., Slutsker, I., Abuhassan, N., Newcomb, W.W., Schafer, J.S., Chatenet, B., Lavenu, F., Kaufman, Y.J., Castle, J.V., Setzer, A., Markham, B., Clark, D., Frouin, R., Halthore, R., Karneli, A., O'Neill, N.T., Pietras, C., Pinker, R.T., Voss, K., Zibordi, G.. An emerging ground-based aerosol climatology: Aerosol optical depth from aeronet. Journal of Geophysical Research: Atmospheres 2001;106(D11):12067-12097. URL: https://agupubs.onlinelibrary.wiley.com/doi/abs/10.1029/2001JD900014.

doi:https://doi.org/10.1029/2001JD900014.
arXiv:https://agupubs.onlinelibrary.wiley.com/doi/pdf/10.1029/2001JD900014.

Hu, Y., Zang, Z., Chen, D., Ma, X., Liang, Y., You, W., Pan, X., Wang, L., Wang, D., Zhang, Z.. Optimization and evaluation of so2 emissions based on wrf-chem and 3dvar data assimilation. Remote Sensing 2022;14(1). URL: https://www.mdpi.com/2072-4292/14/1/220. doi:10.3390/rs14010220.

Kaufman, Y.J., Holben, B.N., Tanré, D., Slutsker, I., Smirnov, A., Eck, T.F.. Will aerosol measurements from terra and aqua polar orbiting satellites represent the daily aerosol abundance and properties? Geophys Res Lett 2000;27:23:3861-3864. doi:10.1029/2000GL011968.

Kumar, U., De Ridder, K., Lefebvre, W., Janssen, S.. Data assimilation of surface air pollutants (o_3 and no_2) in the regionalscale air quality model aurora. Atmos Env 2012;60:99-108. URL: https://doi.org/10.1016/j.atmosenv.2012.06.005. doi:10.1016/j.atmosenv.2012.06.005.

Lee, E.H., Ha, J.C., Lee, S.S., Chun, Y.. Pm10 data assimilation over south korea to asian dust forecasting model with the optimal interpolation method. Asia-Pacific Journal of Atmospheric Sciences 2013;49:73-85. URL:

https://www.semanticscholar.org/paper/PM10-data-assimilation-over-south-Korea-to doi:10.1007/s13143-013-0009-y.

Liang, Y., Zang, Z., Liu, D., Yan, P., Hu, Y., Zhou, Y., You, W.. Development of a three-dimensional variational assimilation system for lidar profile data based on a size-resolved aerosol model in wrf-chem model v3.9.1 and its application in $pm_{2.5}$ forecasts across china. Geoscientific Model Development 2020;13(12):6285-6301. URL: https://gmd.copernicus.org/articles/13/6285/2020/. doi:10.5194/gmd-13-6285-2020.

Loosmore, A.. Evaluation and development of models for resuspension of aerosols at short times after deposition. Atmos Env 2003;37:639-647. doi:10.1016/S1352-2310(02)00902-0.

Majdi, M., Turquety, S., Sartelet, K., Legorgeu, C., Menut, L., Kim, Y.. Impact of wildfires on particulate matter in the euro-mediterranean in 2007: sensitivity to the parameterization of emissions in air quality models. Atmos Chem Phys Discuss 2018;2018:1-32. URL: https://www.atmos-chem-phys-discuss.net/acp-2018-309/. doi:10.5194/acp-2018-309.

Menut, L., Bessagnet, B., Khvorostyanov, D., Beekmann, M., Blond, N., Colette, A., Coll, I., Curci, G., Foret, G., Hodzic, A., Mailler, S., Meleux, F., Monge, J.L., Pison, I., Siour, G., Turquety, S.,

Valari, M., Vautard, R., Vivanco, M.G.. Chimere 2013: a model for regional atmospheric composition modelling. Geosci Model Dev 2013;6(4):981-1028. URL: https://www.geosci-model-dev.net/6/981/2013/. doi:10.5194/gmd-6-981-2013.

Monahan, E.C., Spiel, D.E., Davidson, K.L.. A model of marine aerosol generation via whitecaps and wave disruption. In: Oceanic whitecaps and their role in air-sea exchange processes. D. Reidel, Netherlands; 1986. p. 167-174.

Nilsson, E.D., Rannik, U., Buzorius, G., Kulmala, M., OâĂŹDowd, C.. Effects of the continental boundary layer evolution, convection, turbulence and entrainment on aerosol formation. Tellus B 2001;53:441âĂŞ461.

Pagowski, M., Grell, G.A.. Experiments with the assimilation of fine aerosols using an ensemble kalman filter. Journal of Geophysical Research: Atmospheres 2012;117(D21). URL: https://agupubs.onlinelibrary.wiley.com/doi/abs/10.1029/2012JD018333. doi:https://doi.org/10.1029/2012JD018333. arXiv:https://agupubs.onlinelibrary.wiley.com/doi/pdf/10.1029/2012JD018333.

Pandis, S.N., Wexler, A.S., Seinfeld, J.H.. Secondary organic aerosol formation and transport ii. predicting the ambient secondary organic aerosol size distribution. Atmos Env 1993;27A. doi:10.1016/0960-1686(93)90408-Q.

Park, R.S., Song, C.H., Han, K.M., Park, M.E., Lee, S.S., Kim, S.B., Shimizu, A.. A study on the aerosol optical properties over east asia using a combination of cmaq-simulated aerosol optical properties and remote-sensing data via a data assimilation technique. Atmos Chem Phys 2011;11(23):12275-12296. URL: https://www.atmos-chem-phys.net/11/12275/2011/. doi:10.5194/acp-11-12275-2011.

Prank, M., Sofiev, M., Tsyro, S., Hendriks, C., Semeena, V., VazhappillyÃĆ Francis, X., Butler, T., DenierÃĆ vanÃĆ derÃĆ Gon, H., Friedrich, R., Hendricks, J., Kong, X., Lawrence, M., Righi, M., Samaras, Z., Sausen, R., Kukkonen, J., Sokhi, R.. Evaluation of the performance of four chemical transport models in predicting the aerosol chemical composition in europe in 2005. Atmos Chem Phys 2016;16(10):6041-6070. URL: https://www.atmos-chem-phys.net/16/6041/2016/. doi:10.5194/acp-16-6041-2016.

Roustan, Y., Sartelet, K., Tombette, M., Debry, É., Sportisse, B.. Simulation of aerosols and gas-phase species over Europe with the Polyphemus system. Part II: Model sensitivity analysis for 2001. Atmos Env 2010;44(34):4219-4229. doi:10.1016/j.atmosenv.2010.07.005.

Sandu, I., Stevens, B., Pincus, R.. On the

transitions in marine boundary layer cloudiness.
Atmos Chem Phys 2010;10(5):2377-2391. URL:
https://www.atmos-chem-phys.net/10/2377/2010/.
doi:10.5194/acp-10-2377-2010.

Schwartz, C.S., Liu, Z., Lin, H.C., Cetola, J.D..
Assimilating aerosol observations with a âĂIJhybridâĂİ
variational-ensemble data assimilation system.
J Geophys Res Atmos 2014;119:4043-4069. URL:
https://agupubs.onlinelibrary.wiley.com/doi/full/10.1002/2013JD020937.
doi:https://doi.org/10.1002/2013JD020937.

Segers, A.. Data assimilation in atmospheric chemistry models
using Kalman filtering. PhD thesis 2002;doi:Delft Univ.,
Delft, Netherlands.

Sekiya, T., Miyazaki, K., Ogochi, K., Sudo, K.,
Takigawa, M., Eskes, H., Boersma, K.F.. Impacts
of horizontal resolution on global data assimilation
of satellite measurements for tropospheric chemistry
analysis. Journal of Advances in Modeling
Earth Systems 2021;13(6):e2020MS002180. URL:
https://agupubs.onlinelibrary.wiley.com/doi/abs/10.1029/2020MS002180.
doi:https://doi.org/10.1029/2020MS002180.
arXiv:https://agupubs.onlinelibrary.wiley.com/doi/pdf/10.1029/2020MS002180;
e2020MS002180 2020MS002180.

Stern, R., Builtjes, P., Schaap, M., Timmermans,

R., Vautard, R., Hodzic, A., Memmesheimer, M., Feldmann, H., Renner, E., Wolke, R., Kerschbaumer, A.. A model inter-comparison study focussing on episodes with elevated pm10 concentrations. Atmospheric Environment 2008;42(19):4567-4588. URL: https://www.sciencedirect.com/science/article/pii/S1352231008001179. doi:https://doi.org/10.1016/j.atmosenv.2008.01.068.

Tang, Y., Chai, T., Pan, L., Lee, P., Tong, D., Kim, H.C., Chen, W.. Using optimal interpolation to assimilate surface measurements and satellite aod for ozone and $pm_{2.5}$: A case study for july 2011. J AIR WASTE MANAGE 2015;65:10:1206-1216. doi:10.1080/10962247.2015.1062439.

Tang, Y., Pagowski, M., Chai, T., Pan, L., Lee, P., Baker, B., Kumar, R., Delle Monache, L., Tong, D., Kim, H.C.. A case study of aerosol data assimilation with the community multi-scale air quality model over the contiguous united states using 3d-var and optimal interpolation methods. Geosci Model Dev 2017;10(12):4743-4758. URL: https://www.geosci-model-dev.net/10/4743/2017/. doi:10.5194/gmd-10-4743-2017.

Terrenoire, E., Bessagnet, B., Rouïl, L., Tognet, F., Pirovano, G., Létinois, L., Beauchamp, M., Colette, A., Thunis, P., Amann, M., Menut, L.. High-resolution air quality simulation over

europe with the chemistry transport model chimere. Geoscientific Model Development 2015;8(1):21-42. URL: https://gmd.copernicus.org/articles/8/21/2015/. doi:10.5194/gmd-8-21-2015.

Thiébaux, H.J., Pedder, M.A.. Spatial objective analysis: With applications in atmospheric science. Academic Press 1987;.

Tombette, M., Mallet, V., Sportisse, B.. Pm_{10} data assimilation over europe with the optimal interpolation method. Atmos Chem Phys 2009;9(1):57-70. URL: https://www.atmos-chem-phys.net/9/57/2009/. doi:10.5194/acp-9-57-2009.

Van Loon, M., Roemer, M., Builtjes, P.. Model intercomparison in the framework of the review of the Unified EMEP model. Tech rep 2004;TNO Environment Energy and Process Innovation, TNO report âĂŞ R2004/282.

Wang, Y., Sartelet, K.N., Bocquet, M., Chazette, P.. Assimilation of ground versus lidar observations for pm_{10} forecasting. Atmos Chem Phys 2013;13(1):269-283. URL: https://www.atmos-chem-phys.net/13/269/2013/. doi:10.5194/acp-13-269-2013.

Wesely, M.. Parameterization of surface resistances to gaseous

dry deposition in regional-scale numerical models. Atmos Env 1989;23(6):1293-1304. doi:10.1016/j.atmosenv.2007.10.058.

Wu, L., Mallet, V., Bocquet, M., Sportisse, B.. A comparison study of data assimilation algorithms for ozone forecasts. J Geophys Res 2008;113:D20310. doi:10.1029/2008JD009991.